Available online at www.sciencedirect.com
ScienceDirect
Journal of Nuclear Materials 371 (2007) 107–117
journal of nuclear materials
www.elsevier.com/locate/jnucmat

Effect of irradiation on stress corrosion cracking in supercritical water

S. Teysseyre *, Z. Jiao, E. West, G.S. Was

Nuclear Engineering and Radiological Sciences, University of Michigan, 2355 Bonisteel Boulevard, Ann Arbor, MI 48109, United States

Abstract

Proton irradiation was used to study the effect of irradiation on stress corrosion cracking of 316L stainless steel and nickel-base alloy 690 in supercritical water (SCW). Irradiation to 7 dpa at 400 °C and 500 °C resulted in increased stress corrosion cracking (SCC) in SCW over the unirradiated case with the severity increasing with temperature. Irradiation results in significant radiation-induced segregation, formation of dislocation loops and voids (at 500 °C) and hardening. Neither RIS nor irradiation hardening correlates with SCC susceptibility.

1. Introduction

Stress corrosion cracking (SCC) behavior of austenitic alloys in supercritical water has showed that many alloys (304, 316, 316L, 347) experience some degree of stress corrosion cracking, most of which is intergranular [1–3]. Most results show intergranular cracking on the gage surface even when intergranular cracking is not observed on the fracture surface. Nickel-base alloy 718 proved to be extremely susceptible to SCC [4]. The authors attributed this cracking behavior to the oxidation and swelling of the primary niobium carbides that cause cracks to initiate at these carbides. Alloy 625 also exhibited high susceptibility to intergranular stress corrosion cracking [3] while one study [4] showed that alloy 690 was resistant to intergranular stress corrosion cracking (IGSCC), Teysseyre and Was [3] found evidence of IGSCC in this alloy at 400, 450, 500 and 500 °C, with the extent of cracking increasing with temperature. Limited tests have also been conducted on alloy 800H that exhibited evidence of brittle fracture over a portion of the fracture surface [5].

Perhaps the most challenging problem is the role of irradiation on the microstructure and how these changes affect stress corrosion cracking. Irradiation assisted stress corrosion cracking has been a generic problem in light water reactors of all types and covering many austenitic and nickel-base alloys [6]. The acceleration of cracking is believed to be related to the effects of irradiation in austenitic alloys: radiation-induced segregation (RIS), microstructure changes (dislocation loops, dislocation network, voids, bubbles, precipitates) and hardening. In austenitic alloys, RIS leads to chromium depletion and nickel enrichment at grain boundaries. The segregation profile is very narrow, generally between 5 and 10 nm, and increases with neutron

* Corresponding author. Fax: +1 734 763 4540.
E-mail address: teysseyr@umich.edu (S. Teysseyre).

0022-3115/$ - see front matter © 2007 Elsevier B.V. All rights reserved.
doi:10.1016/j.jnucmat.2007.05.008

dose. A possible cause for increased cracking with dose is chromium depletion that leads to higher susceptibility of grain boundaries for cracking. However, work by Busby [7] shows that RIS alone cannot be responsible for the increase of cracking. The microstructure of austenitic alloys changes rapidly under irradiation to produce features as dislocation loops, dislocation network, voids and precipitates. Around 300 °C, the irradiated microstructure is dominated by Frank dislocation loops. Loop density saturates very quickly (1 dpa) whereas loop diameter increases until about 3–5 dpa. As temperature increases, voids and bubbles are created and a dislocation network develops. A consequence of irradiation-induced changes is hardening of the alloy. As dose increases, yield strength increases following a square root dose dependence. Hence, an irradiated stainless steel may see yield strength increases up to five times after 7–10 dpa. Hardening is also considered as a primary factor in IASCC susceptibility. Hardening due to cold work is known to cause an increase of crack growth rate in austenitic stainless steel strained in 288 °C BWR normal water [8]. Increased yield strength due to irradiation also correlates with an increase of IASCC susceptibility [9]. Such evidence suggests that hardening is a key factor in IASCC susceptibility. However, it has been observed that microstructure changes not only affect the hardening but also the deformation mode. With dose, deformation becomes heterogeneous as plasticity becomes localized in channels [10]. It has been suggested that microstructure itself and not just the hardness is responsible for IASCC [11].

To date, no data exist on the role of irradiation on SCC in a supercritical water environment. The main difference between the SCWR and currents LWRs is the temperature range. With core structural material temperatures expected to reach 600 °C, the irradiated microstructure will be more similar to that in a fast reactor: RIS at a maximum, hardening is reduced, void formation and, perhaps, radiation-induced precipitation will occur. The purpose of this paper is to determine the effect of irradiation on the SCC susceptibility of 316L SS and alloy 690 and to relate changes in susceptibility to changes in microstructure.

2. Experiment

2.1. Materials

Two commercial purity alloys were used for this study: stainless steel alloy 316L (UNS S31603) and nickel-base alloy 690 (UNS N06690). Both 316L and 690 are used for core internal components in light water reactors and are candidate alloys for the supercritical water-cooled reactor concept. The measured composition of the alloys is shown in Table 1. Alloy 316L was solution annealed at 1100 °C for 20 min and water quenched to prevent carbide formation, resulting in a grain size of 44 μm. Alloy 690 in the as-received condition had an extremely non-uniform grain size distribution. To produce a more uniform grain size, the as-received material was deformed to 66% and then heat treated at 1100 °C for 2 h, resulting in a grain size of 20 μm. Alloys were machined into tensile samples and TEM bars. Tensile samples have threaded ends and a gage dimension of 2 mm × 2 mm × 23 mm. TEM bars are 2 mm × 2 mm × 20 mm and are used for hardness measurements prior of making TEM disks. Samples were made by electric discharge machining. The machined samples were mechanically polished using standard metallographic techniques and then electropolished in perchloric acid (10%) and methanol solution maintained at −50 °C applying 40 V for 10–20 s to obtain a mirror finish.

2.2. Irradiation

The alloys were irradiated with protons in the Michigan Ion Beam Laboratory at the University of Michigan. Samples were mounted on a specially designed copper stage under high vacuum and irradiated using a general ionex tandetron accelerator. Experimental doses and dose rates were calcu-

Table 1
Chemical compositions (wt%) of alloys

Alloys	C	Mn	Fe	S	Si	Ni	Cr	Mo	Cu	N	Co	P	Other
316L	0.022	1.86	Bal	0.001	0.65	10.12	16.62	2.06	0.24	0.02	0.05	0.03	–
690	0.03	0.18	10.0	0.001	0.03	Bal	29.40	0.01	0.01	NM	NM	NM	0.22 Al 0.34 Ti

NM, not measured.

lated using SRIM2003 [12]. As recommended in ASTM E521-89 [13], a displacement energy of 40 eV was used for all dose calculations. Sample temperature during irradiation was maintained at 400 ± 10 °C and 500 ± 10 °C. Irradiations were performed using 3 MeV up to 7 dpa with a dose rate of approximately 1×10^{-5} dpa/s for displacement energy of 40 eV. Both alloys were irradiated to 7 dpa at 400 ± 10 °C and 500 ± 10 °C, with alloy 690 was also irradiated to 4 dpa at 500 ± 10 °C. The result is a relatively uniform damage rate through the first 35 μm of the total proton penetration depth of ~40 μm. Additional details on the techniques of the proton irradiations can be found in Ref. [14].

2.3. Hardening measurement and microstructure analysis

Radiation-induced hardening was evaluated by Vickers indentation with a 25 g load. This load was used to confine the plastic zone of the indent to the irradiated zone, without sampling the unirradiated material. At least 20 indents were made at room temperature for each irradiation condition. The hardness value of the unirradiated condition was subtracted from that of the irradiated condition to arrive at a hardness increase due to irradiation.

TEM discs were cut from the irradiated TEM bars and were prepared by electropolishing in a 5% perchloric acid and 95% methanol solution at −60 °C for an applied current between 15 and 18 mA. Microstructure was characterized using a JEOL2000FX TEM at the University of Michigan Electron Microbeam Analysis Laboratory. The dominant microstructural features observed for all samples were faulted dislocation loops and voids. Faulted dislocation loops were imaged by the rel-rod technique. The rel-rod dark field images were taken near [0 1 1] beam direction and the voids were imaged under slightly underfocus condition.

Grain boundary composition and composition profiles were measured via STEM/EDS using the JEOL 2010F. In the STEM mode, a probe size of 0.5 nm was used in order to collect composition profiles in a period of 30 s to minimize the effect of drift. The *k*-factors used to convert X-ray signal into composition measurements were calculated for each grain by comparison of EDS-determined matrix intensities to the bulk alloy composition determined independently by electron microprobe analysis. Prior to analysis, all TEM samples were plasma cleaned for 10 min using a Southbay PC150 plasma cleaner in an oxygen/argon plasma to minimize sample contamination during room-temperature analysis. Only grain boundaries aligned edge-on to the electron beam were analyzed and multiple measurements were taken on each grain boundary. During a typical analysis of each grain boundary, composition profiles were taken along a 30 nm line scan crossing the grain boundary in ~1.0 nm steps. In addition to the composition profiles, approximately five spot measurements were taken on each boundary to get grain boundary compositions.

2.4. Stress corrosion cracking experiments

Constant extension rate tensile (CERT) experiments were performed in a closed, flowing water loop. The loop consists of a 4-l autoclave made from nickel-base alloy 625, a high-pressure liquid chromatography (HPLC) pump, a preheater system and a back-pressure regulator for control of the pressure. The water is pressurized by an HPLC metering pump and heated in a convection preheater before it flows into the test vessel. The water under supercritical condition flows back out of the autoclave and is cooled by a tube-in-tube heat exchanger before the pressure is reduced by the backpressure regulator (BPR). The water passes though an ion exchanger before flowing back into the main column. The dissolved oxygen content in deionized water was minimized by bubbling Ar in the water column. The oxygen content and conductivity of the circulating water are measured at room temperature and atmospheric pressure in both the inlet and outlet lines. The temperature is measured in the vessel and the pressure is determined at room temperature in the inlet and outlet lines.

Experiments were conducted under 25 MPa of pressure at the temperature at which the samples were irradiated (400 °C and 500 °C). One sample was tested for each irradiation condition. The deaerated condition resulted in an oxygen concentration below 10 ppb and the conductivity in the outlet water was maintained below 0.1 μS/cm for all tests. The samples were strained at a nominal rate of 3×10^{-7} s^{-1} using a stepping motor. All samples were held in the test environment for 12 h before commencing straining.

After removal from the autoclave, samples were examined by scanning electron microscopy to characterize the cracking on the gage surface. Crack density and crack length were recorded on the gage

surfaces, away from the fracture surface, from pictures taken at a magnification of 250× and used to generate the crack length per unit of sample area. Samples were then cross-sectioned and polished in order to determine the penetration depth of the cracks on both the irradiated and unirradiated sides.

3. Results

3.1. Stress corrosion cracking

For all samples, the irradiated gage section of the samples exhibited more cracking than the unirradiated side. As an example, Fig. 1 shows the difference in cracking observed between alloy 690 irradiated to 7 dpa at 500 °C and in the unirradiated condition. The measure of the extent of cracking for all samples tested is the crack length per unit area shown in Fig. 2. Notice that, as for the rest of this paper, the 7 dpa data obtained for alloy 690 irradiated at 500 °C is presented first for intercomparison purpose. At 400 °C, the cracking susceptibility of 316L irradiated to 7 dpa is 1.1 times higher than that of an unirradiated sample. The susceptibility increased by a factor 2.8 for alloy 690 at 400 °C . At 500 °C, the increase of cracking with irradiation is much greater. Irradiated alloy 316L had a crack length per unit area 6 times than on its unirradiated side. This difference was even higher for alloy 690 as a 7 dpa irradiation increased the amount of cracking by a factor of 48.

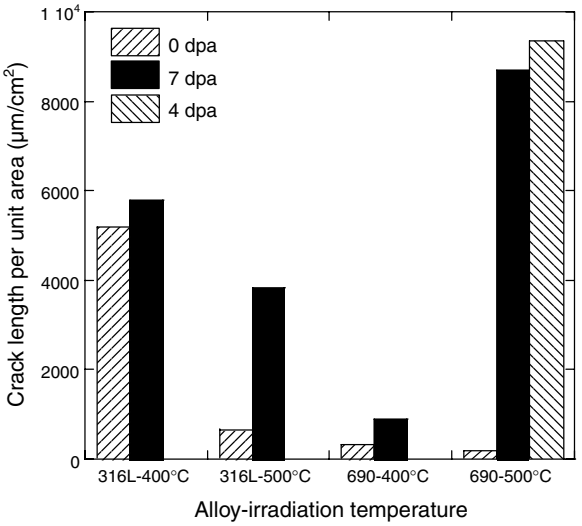

Fig. 2. Influence of irradiation on the cracking susceptibility of alloys 316L and 690 in 400 °C and 500 °C SCW.

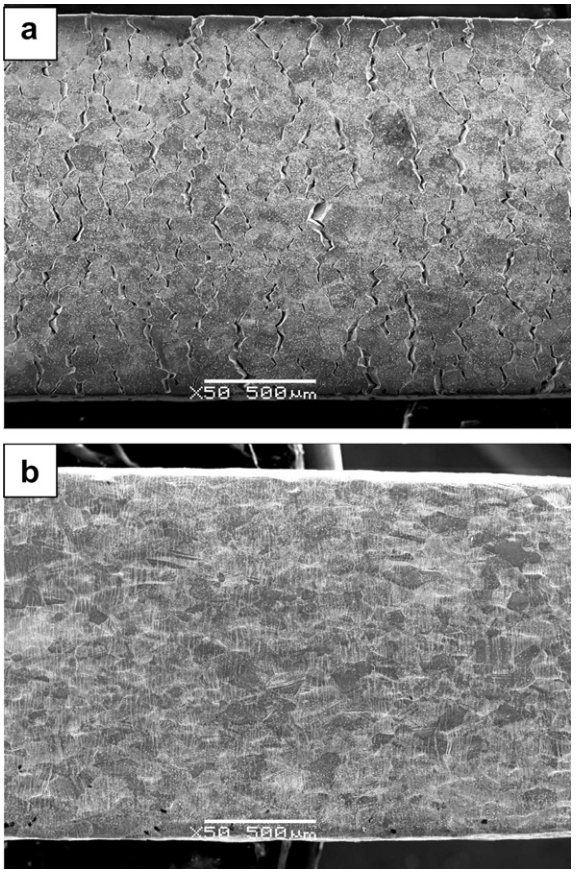

Fig. 1. Gage surface of alloy 690 after completion of CERT test in 500 °C. The irradiated side of the sample irradiated to 7 at 500 °C (a) exhibits more cracks than the unirradiated side (b).

As illustrated in Fig. 3 with the post CERT test cross-section of alloy 690, irradiated to 7 dpa at

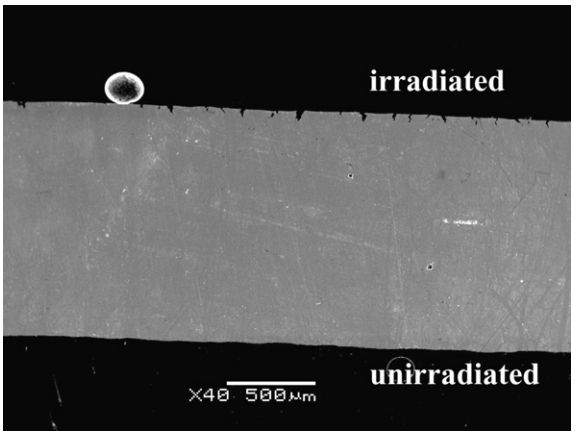

Fig. 3. Cross-section of alloy 690, irradiated to 7 at 500 °C, after completion of CERT test in 500 °C SCW. The cracks that initiated in the irradiated side of the sample propagated deeper in the sample than those in the unirradiated side.

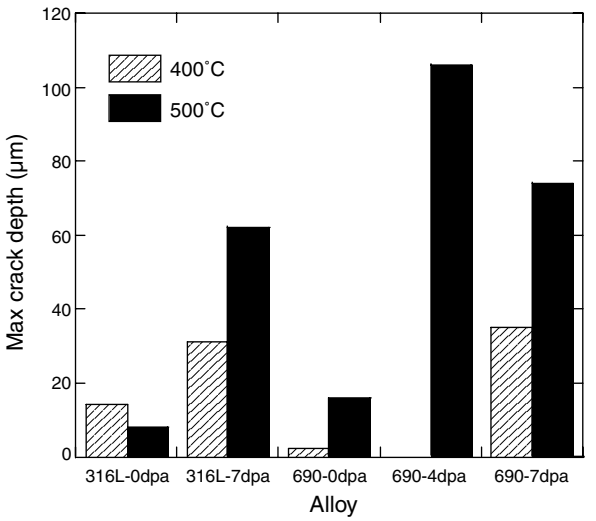

Fig. 4. Influence of irradiation on the crack propagation depth in alloys 316L and 690 in 400 °C and 500 °C SCW.

500 °C, irradiation increased the crack penetration depth. Fig. 4 shows that, at both 400 °C and 500 °C, the maximum crack depth increased with irradiation for both alloys. At 400 °C, the fractional increase in crack depth due to irradiation was greater for the alloy 690 and at 500 °C, the fractional increase in crack depth was greater for 316L. Table 2 presents crack density, average crack length, crack length per unit area and maximum crack depth for both alloys in the unirradiated and irradiated conditions at 400 °C and 500 °C.

3.2. Radiation-induced segregation

Fig. 5 shows an example of the chromium, nickel and iron contents measured across a grain boundary in 316L in the unirradiated state and after 7 dpa at 400 °C and 7 dpa at 500 °C. The average grain boundary concentrations of Cr, Ni and Fe are presented in Fig. 6 and compared with the bulk composition, determined by electron microprobe. The unirradiated sample exhibits a chromium content at the grain boundary of 19 wt% which is greater than the bulk level of 16.8 wt%. The difference is due to chromium enrichment in the steady condition due to thermal non-equilibrium segregation (TNES). This chromium increase is concomitant with iron depletion. The irradiated samples exhibited chromium depletion and nickel enrichment at the grain boundary. After irradiation at 400 °C, chromium at the grain boundary dropped to 14.4 wt% while nickel increased up to 18.9 wt%. At the higher irradiation temperature (500 °C) the depleted zone was slightly wider (±3.5 nm vs ±2.5 nm at 400 °C), and the minimum chromium concentration was slightly lower at 13.8 wt%. A larger temperature effect is observed in the nickel and iron content as nickel concentration increased to 26.5 wt% while iron content decreased 53.7 wt%.

RIS on alloy 690 are presented in Fig. 7 and average grain boundary concentrations are shown in Fig. 8. In addition with doses and irradiation temperatures described for 316L, RIS was also determined on alloy 690 irradiated to 4 dpa at 500 °C. As with 316L, the unirradiated alloy 690 exhibits a sharp chromium segregation enrichment at the grain boundary and iron depletion, likely due to TNES [15]. Irradiation to 7 dpa at 400 °C induced chromium depletion to 18.5 wt% while nickel content increased to 75.6 wt%. As with 316L, the depleted zone is slightly wider after irradiation at 500 °C. The minimum chromium content is lower with 15.2 wt% and the nickel concentration is higher with 78.1 wt%. Dose effect can

Table 2
Results of constant extension rate experiments performed in deaerated SCW (25 MPa,O_2 < 10 ppb, conductivity < 0.1 μS/cm)

Alloy	Irradiation condition	Irradiation and test temperature (°C)	Dose on surface[a] (dpa)	Crack density (#/mm^2)	Average crack length (μm)	Crack length/unit area (μm/mm^2)	Maximum crack depth (μm)
316L	400 °C/	400	0	235	22	5185	14
	7 dpa		7	173	33	5779	31
	500 °C/	500	0	20	33	650	8
	7 dpa		7	77	49	3825	62
690	400 °C/	400	0	25	13	322	2
	7 dpa		7	47	19	898	33
	500 °C/	500	0	10	18	181	16
	7 dpa		7	154	56	8709	74
	500 °C/	500	0	24	34	803	11
	4 dpa		4	143	65	9355	106

[a] The unirradiated side (0 dpa) of the irradiated sample is compared to the irradiated side of the same sample.

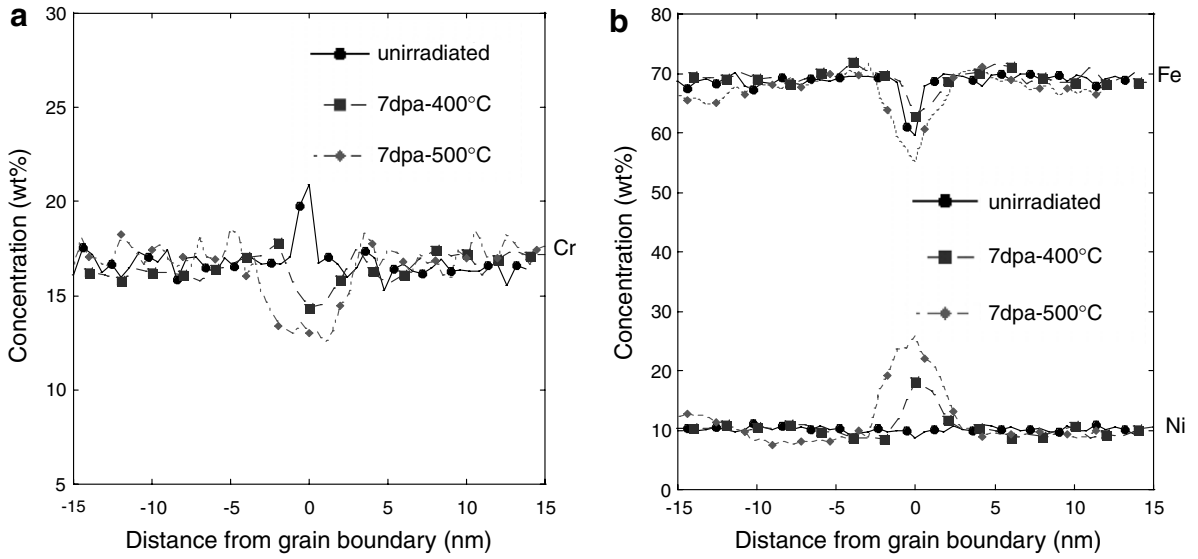

Fig. 5. Element concentration across a grain boundary of alloy 316L unirradiated and irradiated to 7 dpa at 400 and 500 °C (a) Cr, (b) Ni,Fe.

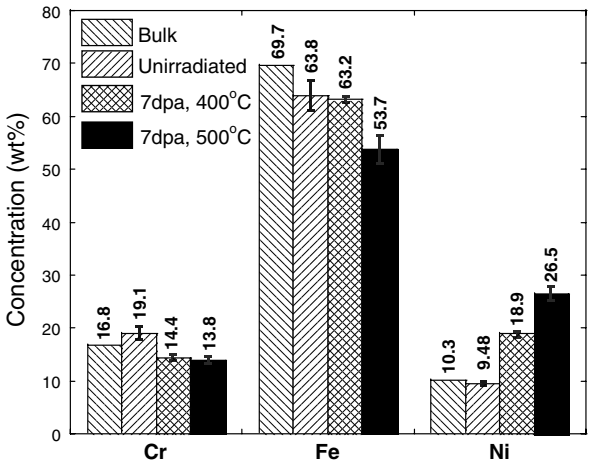

Fig. 6. Grain boundary concentrations of Cr, Ni and Fe for 316L in the nominal state and after 7 dpa at 400 °C and 7 dpa at 500 °C.

be observed by comparing RIS obtained at 4 dpa/500 °C and 7 dpa/500 °C. The depleted zone is similar for both doses. Minimum chromium concentration is 18 wt% and 15.2 wt% at 4 dpa and 7 dpa, respectively.

3.3. Microstructure

Figs. 9 and 10 show some faulted loops and voids observed on both alloys at 400 °C and 500 °C. The microstructure of alloy 316L irradiated at 400 °C to 7 dpa exhibited a large fraction of small loops (7 nm of diameter) as shown in Fig. 11 and no voids. Irradiation at 500 °C generated larger loops (25 nm) and voids appeared. The void size distribution is centered over the 15–20 nm diameter range (Fig. 12). Microstructure changes for alloy 690 followed the same trend, with very small loops (around 3 nm) at 7 dpa/400 °C and no voids, whereas the loop size increased to 20 nm and voids size increased to 10 nm at 7 dpa/500 °C. At 500 °C, a dose increase from 4 dpa to 7 dpa had little effect on the microstructure as loop and void size only increase slightly with dose. Summary of data collected on the microstructure is presented in Table 3.

3.4. Hardening

Irradiation hardening is shown in Fig. 13. Both alloys exhibited noticeable hardening after irradiation. The hardening reaches 237 kg/mm^2 for alloy 316L and 203 kg/mm^2 for 690 at 400 °C. Hardening also occurred during the 500 °C irradiation but to a lesser extent than at 400 °C. Hardening appeared to be slightly less for 690 (101 kg/mm^2) than for 316 L (126 kg/mm^2). Small hardening increase occurred between 4 dpa and 7 dpa at 500 °C for alloy 690. Hardening data collected are presented in Table 3.

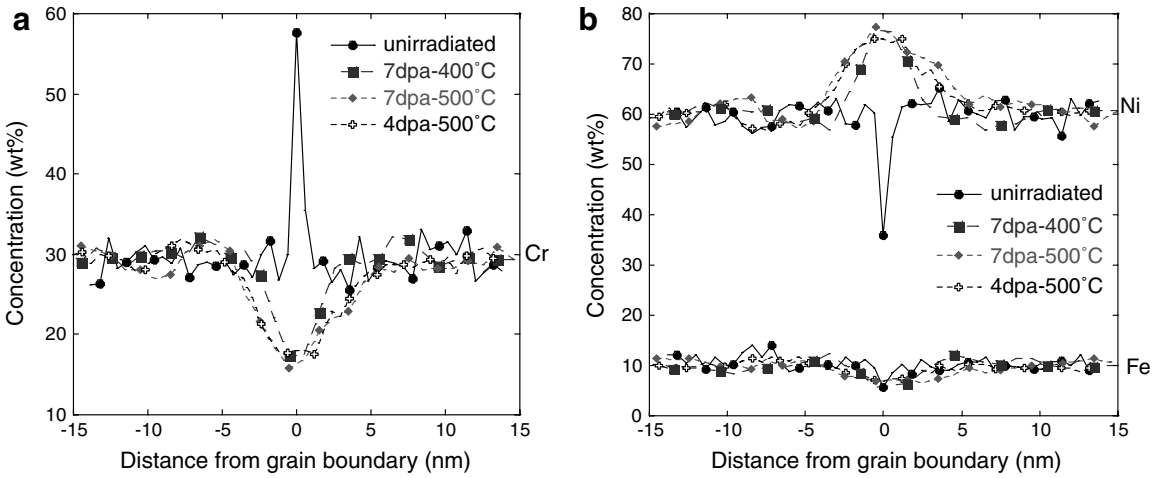

Fig. 7. Element concentration across a grain boundary of alloy 690 unirradiated, irradiated to 7 dpa at 400 and 500 °C and irradiated to 4 dpa at 500 °C (a) Cr, (b) Ni,Fe.

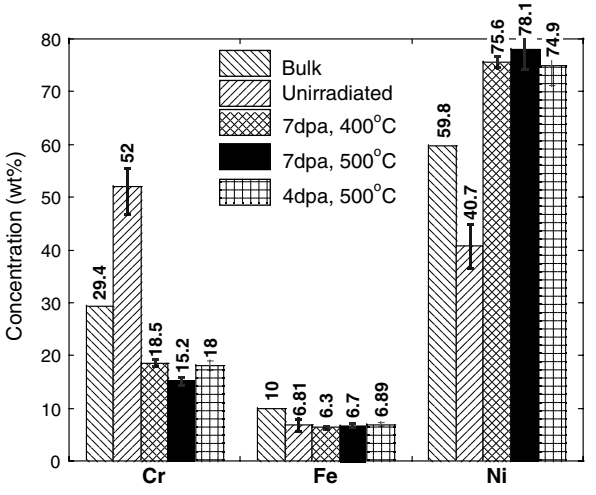

Fig. 8. Grain boundary concentrations of Cr, Ni and Fe for alloy 690 in the nominal state and after 7 dpa at 400 °C and 7 and 4 dpa at 500 °C.

4. Discussion

CERT experiments showed that the alloys irradiated at 400 °C and 500 °C and tested in supercritical water at the irradiation temperature exhibited an increase in cracking over the unirradiated case. Although the limited number of experiments precludes a quantitative analysis, the effect was significantly greater at 500 °C than at 400 °C. The difference was such that alloy 690, considered as more SCC resistant at all temperature in the unirradiated state, and more resistant following irradiation at 400 °C, was shown to be the most susceptible to cracking following irradiation at 500 °C. Before analyzing the cracking behavior in light of the irradiated microstructure, the microstructure is compared to that expected based on the existing literature.

Composition profiles measured along the grain boundaries of irradiated alloys showed that RIS occurred at 400 °C and 500 °C. For alloy 316L, the grain boundary chromium concentration was very similar at both temperatures with slightly more depletion occurring at 500 °C. The difference was slightly higher for alloy 690. In Fe–Ni–Cr alloys, the vacancy exchange or inverse Kirkendall mechanism explains the segregation [16]. RIS calculation based on this mechanism over the temperature range of 200–800 °C shows that the peak in segregation occurs around 500 °C and that segregation is expected to be slightly higher at 500 °C than at 400 °C [17]. The results are therefore consistent with the inverse Kirkendall model prediction and with our current knowledge of the RIS mechanism.

The analysis of the microstructure showed that increasing irradiation temperature tended to increase the loop sizes and to enhance void formation, in agreement with the expected effect of temperature on microstructure [18]. Faulted loop densities obtained are similar to those observed in neutron irradiated stainless steels [19]. Irradiation hardening also follows the expected dependence on temperature with less hardening at higher temperature. Furthermore, calculations based on the dispersed barrier-hardening model indicated that there is a relatively good correlation between

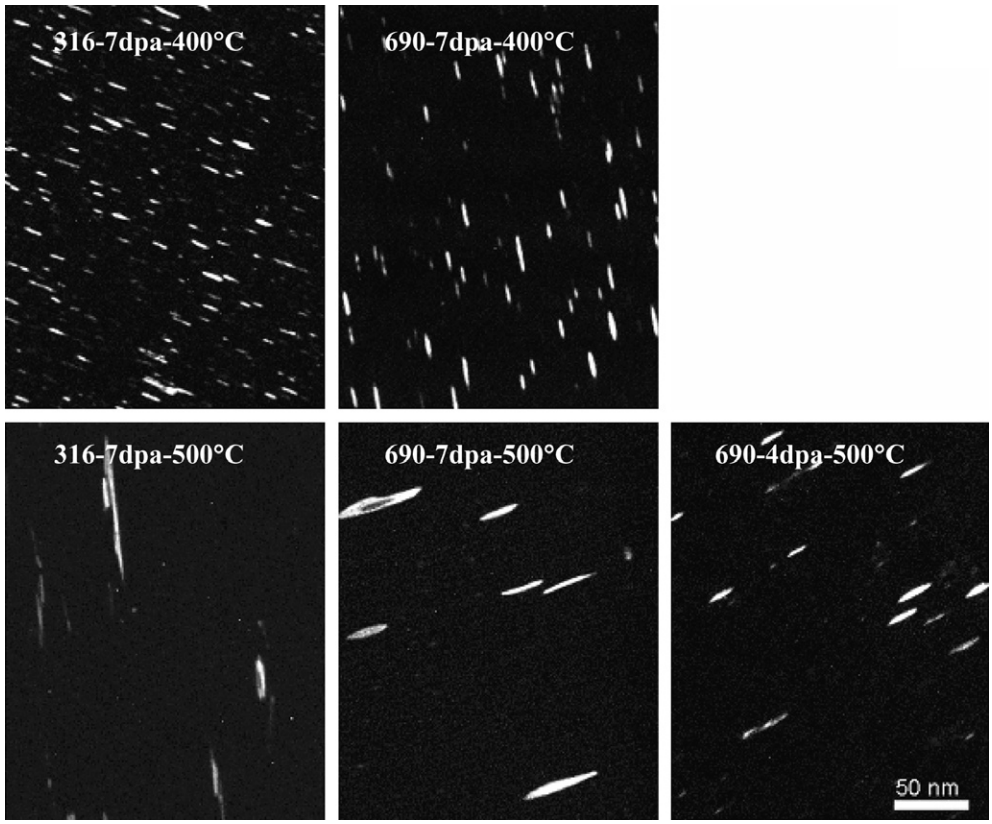

Fig. 9. TEM rel-rod dark field images of faulted loops observed for 316L at 400 °C/7 dpa and 500 °C/7 dpa and for 690 at 400 °C/7 dpa and 500 °C/7 and 4 dpa.

hardening determined from the observed microstructure and the measured hardening (Table 3). The increment of yield strength depends upon the barrier density and size according to the relation [20]:

$$\Delta\sigma_y = M\alpha\mu b(Nd)^{0.5} \quad \text{and}$$
$$\Delta\sigma_{\text{micros}} = [(\Delta\sigma_y^{\text{loop}})^2 + (\Delta\sigma_y^{\text{void}})^2]^{0.5}, \tag{1}$$

where M is the Taylor factor (3.06), α is the barrier strength factor (1.0 for voids, 0.6 for faulted loops), μ is the shear modulus, b is the Burgers vector for the network dislocation, N is the defect number density and d is the mean size of the defects. The shear modulus $\mu = 76$ GPa for 316L and 79 for alloy 690 and $b = 2.5 \times 10^{-8}$ cm. For austenitic steels, the yield strength estimated from the hardening data can be estimated by using the following empirical relation [21]:

$$\Delta\sigma_{H_v} = 3.03\Delta H_V, \tag{2}$$

where ΔH_V is the hardness increment of hardness in kg/mm^2 and $\Delta\sigma_y$ is the yield strength increment in MPa.

The small differences between RIS obtained at 400 °C and 500 °C is unlikely to explain the difference in the extent of cracking in either 316L or 690. Furthermore, it is particularly remarkable that chromium depletion with alloy 690 obtained at 500 °C/4 dpa is very similar to that obtained at 400 °C/7 dpa but there is no correlation with the extent of cracking. Also, it is reasonable to assume that with less than 10 ppb of dissolved oxygen, SCW is a low potential environment in which chromium depletion should not significantly affect the corrosion resistance. There was a clear difference in hardening between 400 °C and 500 °C but higher cracking was obtained at the lower irradiation temperature where hardening was lower. As discussed previously, IASCC in LWRs has been shown to increase with hardening. Whereas SCW is a different environment, it is unlikely that a softer microstructure would promote more cracking than a harder

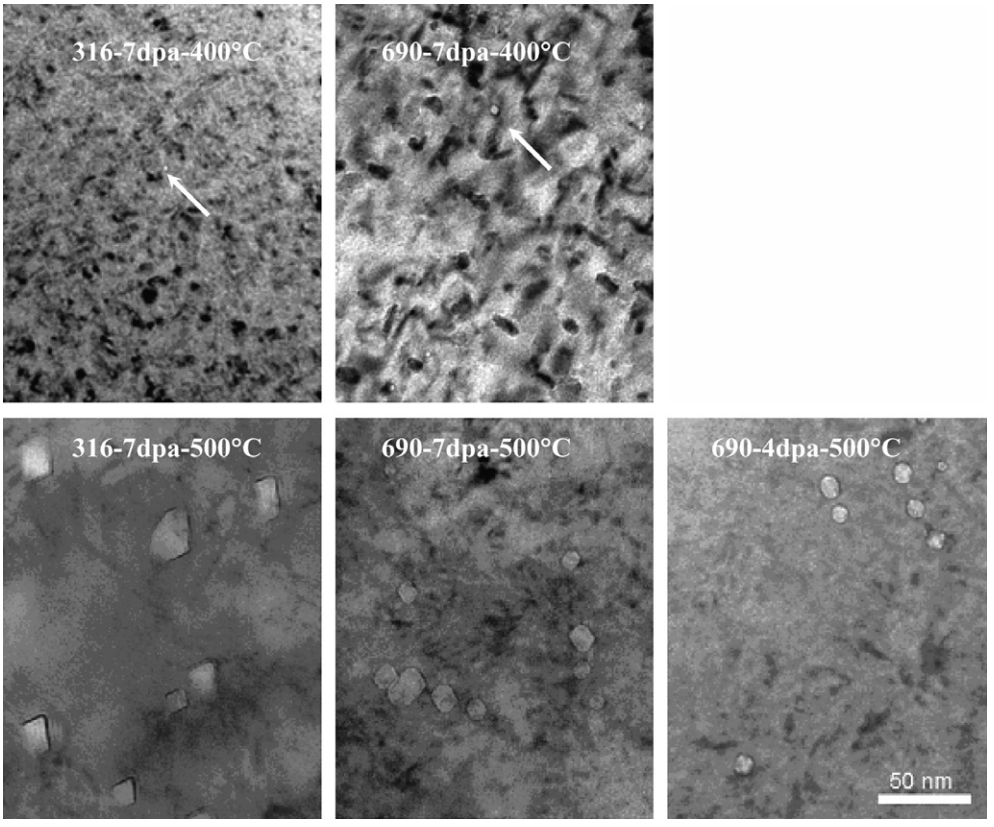

Fig. 10. TEM images of voids for 316L at 400 °C/7 dpa and 500 °C/7 dpa and for 690 at 400 °C/7 dpa and 500 °C/7 and 4 dpa. Arrows indicated voids observed at 400°C.

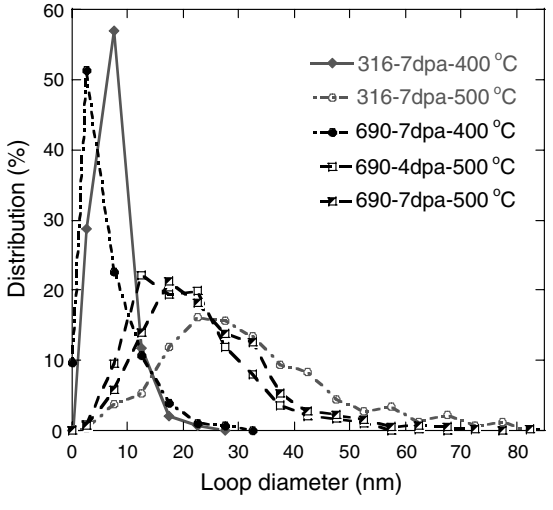

Fig. 11. Loop size distribution for 316L at 400 °C/7 dpa and 500 °C/7 dpa and for 690 at 400 °C/7 dpa and 500 °C/7 and 500 °C/4 dpa.

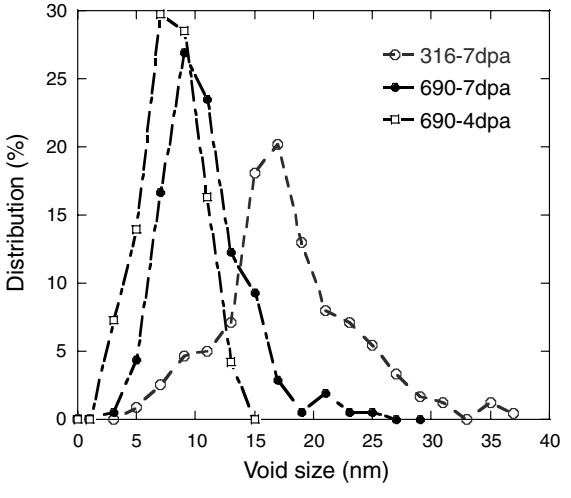

Fig. 12. Void size distribution at 500 °C/7 dpa for 316L and 500 °C/7 dpa and 4 dpa for 690. No voids were observed at 400 °C.

one. Furthermore, it was shown that hardening can be reasonably well accounted for by the microstructure, so the measured values of hardening validate the microstructure measurements. It must

Table 3
Summary of microstructure analysis for 316L and 690

Alloy	Irradiation condition	Loops			Voids			ΔH_v (kg/mm^2)	$\Delta\sigma_{H_v}$ (Mpa)	$\Delta\sigma_{micros}$ (MPa)
		Number of loops measured	Average diameter (nm)	Density (#/cm^3)	Number of voids measured	Average diameter (nm)	Density (#/cm^3)			
316L	400 °C/ 7 dpa	492	6.9	5.3×10^{16}	NA	~2.0	$<10^{14}$	237	718	667
	500 °C/ 7 dpa	322	31.9	3.03×10^{15}	236	19.9	5.14×10^{14}	126	382	390
690	400 °C/ 7 dpa	466	10.2	3.2×10^{16}	NA	~3.0	$\sim10^{14}$	203	639	636
	500 °C/ 7 dpa	614	24.2	3.74×10^{15}	204	10.7	1.51×10^{15}	101	318	405
	500 °C/ 4 dpa	438	20.8	3.62×10^{15}	165	8.0	1.25×10^{15}	96	302	354

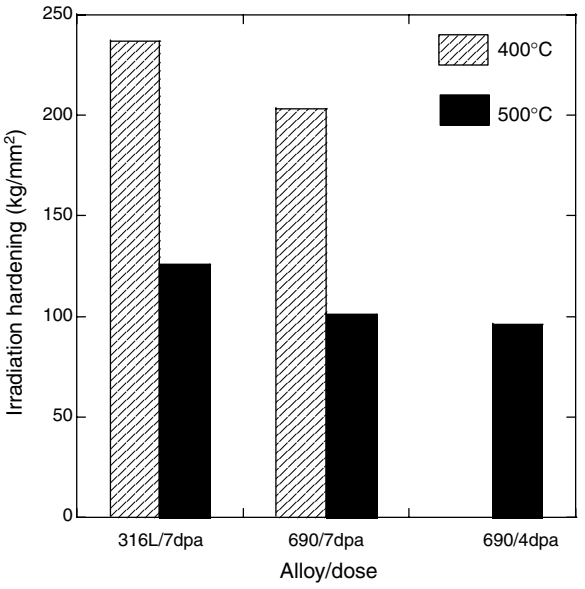

Fig. 13. Hardening of 316L at 400 °C/7 dpa and 500 °C/7 dpa and alloy 690 at 400 °C/7 dpa, 500 °C/7 dpa and 500 °C/4 dpa.

be concluded that neither irradiation hardening nor RIS are the primary factors enhancing IGSCC following irradiation.

In this analysis, the microstructure has been mainly considered for its effect on hardening. However, microstructure can also influence the deformation mode. It is known that dislocation channeling increases with dose [22] and channeling enhances slip localization that may affect cracking. The fact that RIS and hardening cannot explain the greater effect of irradiation at higher temperature may indicate that the deformation mode of the irradiated alloys plays a role.

5. Conclusion

- Irradiation to 7 dpa at 400 °C and 500 °C causes a significant increase in SCC in 316L and alloy 690 as measured by the crack length per unit area on the gage surface and the crack depth measured from cross-sections.
- Irradiation results in grain boundary Cr and Fe depletion and Ni enrichment with the extent of segregation increasing with dose.
- The irradiated microstructure is dominated by small (7 nm) faulted Frank loops at 400 °C and larger Frank loops (25 nm) and voids at 500 °C.
- Irradiation hardening is greater at 400 °C than at 500 °C, in agreement with hardening produced from the microstructure using the dispersed barrier-hardening model. Irradiation hardening is greater on 316L vs alloy 690 at both temperatures.
- Neither RIS nor hardening can satisfactorily account for the changes in SCC susceptibility with irradiation temperature.

References

[1] Y. Tsuchiya, F. Kano, N. Saito, A. Shioiri, S. Kasahara, K. Moriya, H. Takahashi, SCC and Irradiation Properties of Metals under Supercritical-water Cooled Power Reactor Conditions, GENES4/ANP2003, Paper 1096, Kyoto, Japan, September 2003.

[2] R. Fujisawa, K. Nishimura, T. Kishida, M. Sakaihara, Y. Kurata, Y. Watanabe, Cracking Susceptibility of Ni Base Alloys and 316 Stainless Steel in Less Oxidizing or Reducing

SCW, Corrosion 2005, NACE International, Houston, TX, Paper 05395, 2005.
[3] S. Teysseyre, G.S. Was, Corrosion 62 (12) (2006) 1100.
[4] L. Fournier, D. Delafosse, C. Bosch, Th. Magnin, Stress Corrosion Cracking of Nickel Base Superalloys in Aerated Supercritical Water, Corrosion 2001, Paper No. 01361, NACE, Houston, TX, 2001.
[5] J. Jang, in: Presented at the Project Management Board meeting for the SCWR Materials and Water Chemistry, Ann Arbor, MI, March, 2006.
[6] G.S. Was, P. Andresen, JOM 44 (4) (1992) 8.
[7] J.T. Busby, G.S. Was, E.A. Kenik, J. Nucl. Mater. 302 (2002) 20.
[8] M.O. Speidel, R. Magdowski, in: Ford, Brummer, Was (Eds.), Proceedings of the Ninth International Symposium on Environmental Degradation of Materials in Nuclear Power Systems-water Reactors, Metallurgical Society of AIME, Warrendale, PA, 1999, p. 325.
[9] S.M. Brummer, E.P. Simonen, P.M. Scott, P.L. Andresen, G.S. Was, J.L. Nelson, J. Nucl. Mater. 274 (1999) 299.
[10] S.M. Brummer, J. Cole, R. Carter, G.S. Was, in: R.E. Goldand, E.P. Simonen (Eds.), Proceedings of the Sixth International Symposium on Environmental Degradation of Materials in Nuclear Power Systems-water Reactors, TMS, Warrendale, PA, 1993, p. 537.
[11] M.C. Hash, J.T. Busby, G.S. Was, in: M.R. Grossbeck, T.R. Allen, R.G. Lott, A.S. Kumar (Eds.), Proceedings of the 21st International Symposium on Effects of Irradiation on Material, ASTM STP, vol. 1447, American Society for Testing of Material, West Conshohocken, PA.
[12] J.F. Ziegler, J.P. Biersack, SRIM-2003 Program, IBM Corp., Yorktown, NY.
[13] Standard Practice for Neutron Radiation Damage Simulation by Charged-particle Irradiation, ASTM Designation E 521-89, Annual Book of ASTM Standards, vol. 12.02, American Society for Testing and Materials, Philadelphia, PA, 1989, p. D-9.
[14] G. Gupta et al., J. Nucl. Mater 351 (2006) 162.
[15] C.C. Goodwin, R.G. Faulkner, S.B. Fisher, in: R.K. Nanstad, M.L. Hamilton, F.A. Garner, A.S. Kumar (Eds.), Proceedings of the 18th International Symposium, ASTM STP, vol. 1325, ASTM, Philadelphia, 1997.
[16] P.R. Okamoto, L.E. Rehn, J. Nucl. Mater. 83 (1979) 2.
[17] G.S. Was, T. Allen, J. Nucl. Mater 205 (1993) 332.
[18] P.J. Maziasz, C.J. McHargue, Int Mater. Rev. 32 (1987) 190.
[19] S.J. Zinkle, P.J. Maziasz, R.E. Stoller, J. Nucl. Mater. 206 (1993) 266.
[20] A. Seeger, in: Proceedings of the Second United Nations International Conference on Peaceful Uses of Atomic Energy, vol. 6, Geneva, 1958, p. 250.
[21] J.T. Busby, M. Hash, G.S. Was, J. Nucl. Mater 336 (2005) 267.
[22] K. Farrel, T.S. Byun, N. Hashimoto, Mapping Flow Localization Processes in Deformation of Irradiated Reactor Structural Alloys, Oak Ridge National Laboratory, Report ORNL/TM-2002/66, July 2002.